JOURNAL OF SPACECRAFT AND ROCKETS
Vol. 43, No. 6, November–December 2006

Boundary Layer/Streamline Surface Catalytic Heating Predictions on Space Shuttle Orbiter

Jeremiah J. Marichalar* and William C. Rochelle†
Engineering and Science Contract Group (ESCG)/Jacobs Sverdrup, Houston, Texas 77058
and
Benjamin S. Kirk‡ and Charles H. Campbell§
NASA Johnson Space Center, Houston, Texas 77058

DOI: 10.2514/1.23082

This paper describes the analysis of localized catalytic heating effects to the U.S. Space Shuttle Orbiter thermal protection system. The analysis applies to the high-temperature reusable surface insulation on the lower fuselage and wing acreage, as well as the reinforced carbon–carbon on the nose cap, chin panel, and wing leading edge. The objective was to use a modified two-layer approach to predict the catalytic heating effects on the Orbiter windward thermal protection system assuming localized highly catalytic or fully catalytic surfaces. The method incorporated the boundary layer integral matrix procedure–kinetic code with streamline inputs from viscous Navier–Stokes solutions to produce heating rates for localized fully catalytic and highly catalytic surfaces as well as for nominal partially catalytic surfaces (either reinforced carbon–carbon or reaction cured glass) with temperature-dependent recombination coefficients. The highly catalytic heating results showed very good correlation with Orbiter experiments STS-2, -3, and -5 centerline and STS-5 wing flight data. Recommended catalytic heating factors were generated for use in future shuttle missions to perform quick-time atmospheric reentry analysis of damaged or repaired thermal protection system areas. The catalytic factors are presented along streamlines and as a function of stagnation enthalpy for use with arbitrary shuttle trajectories.

Nomenclature

b	=	bump factor equal to ratio of local catalytic to nominal heating rate
C_i	=	mass fraction of ith species
D_{ij}	=	multicomponent diffusion coefficient
$(\hat{e}_\xi, \hat{e}_\eta, \hat{e}_\zeta)$	=	streamline coordinate-aligned unit vectors
H_{cl}	=	arcjet nozzle centerline enthalpy, J/kg
H_w	=	wall enthalpy, J/kg
h^0	=	enthalpy of formation, J/kg
h_{arc}	=	heating parameter
$(\hat{i}, \hat{j}, \hat{k})$	=	Cartesian-aligned unit vectors
L	=	Orbiter reference length, m
M_i	=	normal mass flux of ith species, $\text{kg/m}^2 \cdot \text{s}$
P_{meas}	=	measured test article surface pressure, N/m^2
q	=	heat flux per unit area, W/m^2
r	=	position vector, m
T	=	temperature, K
t	=	time, s
(u, v, w)	=	Cartesian velocity components, m/s
V	=	velocity vector, m/s
(Xo, Yo, Zo)	=	axial, lateral, and vertical shuttle coordinates, m
x	=	Orbiter axial distance from apex, m
(x, y, z)	=	Orbiter Cartesian axis system, m
β	=	chemical energy accommodation coefficient
γ	=	catalytic recombination rate coefficient
ϵ	=	emissivity
λ	=	thermal conductivity, $\text{W/m}^2 \cdot \text{K}$
(ξ, η, ζ)	=	streamline coordinate system
ρ	=	density, kg/m^3
σ	=	Stefan–Boltzmann constant (5.67×10^{-8} $\text{W/m}^2 \cdot \text{K}^4$)

Presented as Paper 180 at the 44th AIAA Aerospace Sciences Meeting and Exhibit, Hilton Casino in Reno, Nevada, 9–12 January 2006; received 8 February 2006; revision received 2 June 2006; accepted for publication 24 July 2006.

*Aerothermal Engineer, Aerothermal and Flight Dynamics, 2224 Bay Area Boulevard, Mailcode JE 5WA.

†Project Manager, Aerothermal and Flight Dynamics, 2224 Bay Area Boulevard, Mailcode JE 5WC. Associate Fellow AIAA.

‡Aerospace Engineer, Applied Aerosciences and CFD Branch, 2101 NASA Parkway, Mailcode EG3.

§Orbiter Aerothermal NASA Subsystem Engineer, Applied Aerosciences and CFD Branch, 2101 NASA Parkway, Mailcode EG3. Senior Member AIAA.

I. Introduction

THE capability to analyze the catalytic heating effects of localized repaired or damaged surfaces on the thermal protection system (TPS) of the U.S. Space Shuttle Orbiter was a major recommendation set forth by the Columbia Accident Investigation Board [1] before the Orbiter could be returned to flight. Because exposed underlying layers of material resulting from damage to the TPS surface can have different thermochemical properties from the reaction cured glass (RCG) coating on the Orbiter windward acreage and/or the reinforced carbon–carbon (RCC) on the wing leading edge, the chemical surface heating, or catalytic heating, occurring during Orbiter atmospheric reentry can significantly increase in the localized damage area beyond the values predicted for flow in chemical equilibrium. In addition, any repair to the TPS may cause a change in the chemical makeup of the repair site, which can also cause higher catalytic heating compared to the surrounding TPS. To incorporate localized catalytic heating overshoots into the shuttle TPS thermal math models, catalytic heating amplification (or bump) factors will be used to increase the nominal heating rates to damaged or repaired areas. These factors are defined as the ratio of the local (overshoot) fully catalytic or highly catalytic heating rate to the nominal, or partially catalytic, heating rate at the same location.

In support of return to flight (RTF), the National Aeronautics and Space Agency (NASA) at Johnson Space Center (JSC) in Houston, Texas requested that analyses be performed to assess the localized

heating effects from highly catalytic surfaces that may be present on the Orbiter TPS during atmospheric reentry. In the event that the Orbiter becomes damaged and must reenter the atmosphere with TPS damage exposure or repair sites, a quick surface heating analysis must be performed to determine if aerothermal heating will become problematic. Because of the lack of catalytic material test data and because performing parametric analyses of catalytic heating solutions in localized areas with computational fluid dynamics (CFD) models is time and resource intensive, a modified two-layer approach consisting of streamline inputs derived from chemical nonequilibrium Navier–Stokes solutions and a boundary layer method was used to perform the analyses. The analyses were compared to the limited amount of catalytic flight data obtained from the Orbiter experiments (OEX) program [2–4].

The objective of the analyses was to ascertain whether the thermochemical kinetic gas model contained in the boundary layer integral matrix procedure—kinetic (BLIMPK) code [5] could be used to predict the catalytic heating rate overshoots exhibited in the OEX program flight measurements with temperature-dependent recombination coefficients from material data analyses of RCG [6] and C742 [7] coated tile. Early BLIMPK analyses used parametrically adjusted constant recombination rates to match the radiometer flight temperature data at the Orbiter stagnation point [8]. Later analyses for the shuttle entry air data system (SEADS) nose cap revealed that localized catalytic surfaces could produce heating rates that overshoot the theoretical fully catalytic (equilibrium) values [9]. Additional observations of this overshoot phenomenon were also documented in other shuttle analyses [10]. If the modified two-layer method could be validated, it would be used to assess surface catalytic heating effects to damaged or repaired TPS locations on the Orbiter during atmospheric reentry in support of RTF recommendations assuming a localized fully catalytic damage site.

II. Methodology

The surface catalytic heating study presented in this paper was conducted over approximately two years and included research of historical flight data and analyses, arcjet tests on coated and uncoated high-temperature reusable surface insulation (HRSI) tiles and RCC materials, a study of analytical approaches, and a large number of new analyses with modified analytical methods and procedures. The following sections describe the progression of the catalytic heating study and the methods employed to develop a working analytical model for obtaining localized catalytic heating factors on a damaged or repaired Orbiter heat shield.

A. Analysis of Flight Data

The first study of catalytic heating factors for use on damaged or repaired locations on the shuttle TPS began in late 2003. Because no measurements of surface catalysis had been obtained for the TPS repair materials or damaged TPS material, existing flight data from early space transportation system (STS) missions, which had highly catalytic C742 coatings on selected HRSI tiles, were used to obtain catalytic heating factors that could be applied to the Orbiter windward TPS [11]. The C742 coatings were placed on two selected tiles along the Orbiter centerline for STS-2 and STS-3. STS-5 contained C742 coated tiles at six centerline locations and two wing locations as indicated in Fig. 1 [2–4].

During these early shuttle flights, a unique phenomenon occurred when the flow passed from the partially catalytic RCG-coated tiles to tiles with the highly catalytic C742 coating. The heating rates on the highly catalytic tiles as obtained from measured thermocouple data increased sharply above the nominal (and surrounding) partially catalytic values and even increased above the heating rate values predicted for fully catalytic or equilibrium flow. Heating rate predictions from the BLIMPK code for flights STS-2, -3, and -5 have been documented that show this overshoot phenomenon [10,12–15]. The overshoot is caused by a sudden drop in oxygen atom (O) concentration at the edge of the highly catalytic surface, with a consequent sudden increase in the oxygen molecule (O_2) concentration. This causes a sudden release of dissociation energy

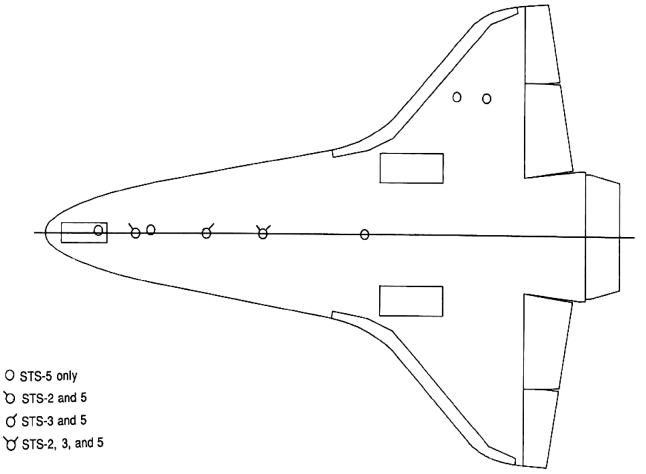

Fig. 1 C742 catalytic tile locations on STS-2, -3, and -5.

and increased heating to the edge of the highly catalytic tile. The heating then drops gradually across the highly catalytic tiles and drops sharply again as the flow then passes over the next partially catalytic tile.

This phenomenon is not limited to tiles, but is documented for flow over the Orbiter RCC nose cap in which the SEADS pressure ports were installed. These ports were made of highly catalytic columbium metal. The sudden increase of the chemical heating rate from the partially catalytic RCC surface as computed by the BLIMPK code over the columbium ports was explained by the sudden drop in atomic oxygen at the wall. After the flow passed the port, the oxygen atom concentration increased back to its nominal level over the RCC, and the heating was reduced to the lower catalytic value. The heating rate then alternately increased and decreased over each port in a sawtooth fashion [9].

The objective of this first catalytic heating study was to use the STS OEX flight data to determine catalytic heating factors by comparing the heating rates of HRSI tiles with the highly catalytic C742 coating to heating rates of the partially catalytic tiles with the original RCG coating. The study was based on the development flight instrumentation data [2–4], which contained the measurements from STS-2, -3, and -5.

Recommended catalytic heating factors were defined for the Orbiter nose cap and chin panel region and the wing leading edge based on the catalytic factors derived from this study of STS-2, -3 and -5 OEX flight data. These factors were later used to perform thermal analyses on the Orbiter RCC panels by the Boeing thermal group that supports the Shuttle Orbiter leading edge structural subsystem (LESS)/RCC problem resolution team (PRT).

B. Arcjet Data

A search was made for previous (historical) data at the JSC arcjet facility as well as for more recent data obtained in the past year. This section describes some of the data which were converted into catalytic factors for a range of enthalpies.

An assessment of wall temperature was made between coated and uncoated RCC test articles tested downstream of the exit of a conical nozzle in the JSC arcjet test position 2 (TP2) [16]. These test data were generated in 1990–1991 and were reported for uncoated RCC [17] and for coated RCC [18,19]. Unfortunately, the test conditions were not the same between the uncoated and coated test articles. However, the data for the coated articles can be extrapolated back to lower values using the heating parameter

$$h_{\text{arc}} = \sqrt{P_{\text{meas}}}(H_{\text{cl}} - H_w) \tag{1}$$

which has been used to correlate surface heat transfer [16]. The required surface temperatures were measured with a laser pyrometer at two conditions of stagnation enthalpy for uncoated RCC and coated RCC. Catalytic (or bump) factors of 1.50–1.55 were

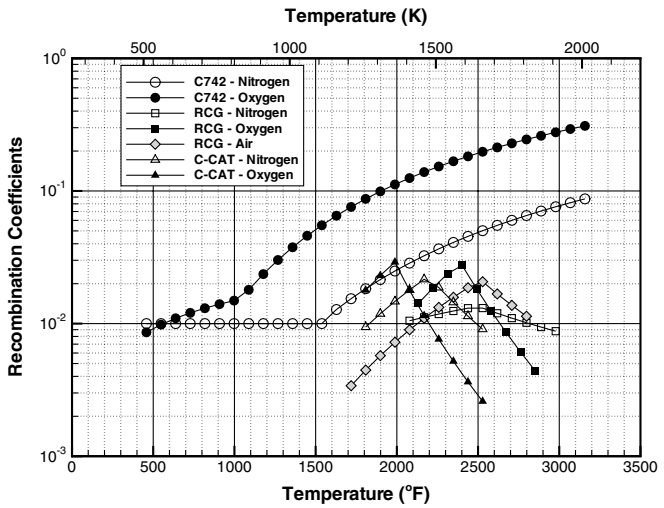

a) Recombination coefficients vs. temperature

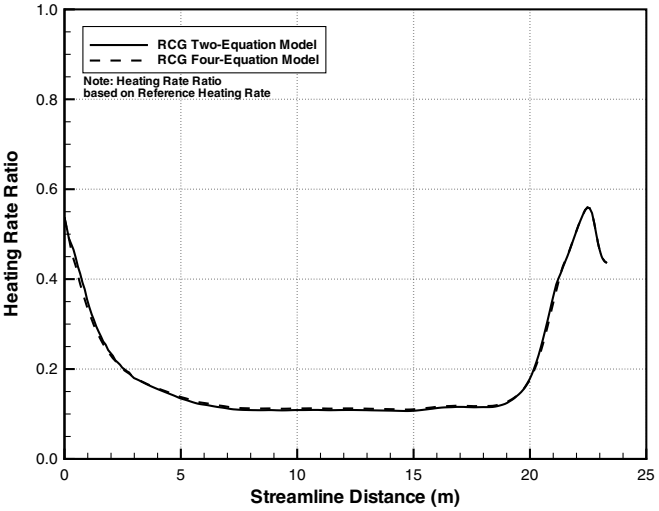

b) Comparison between two and four-equation RCG recombination models

Fig. 2 Recombination coefficients and impact on heat transfer.

calculated [20] from the following equation, assuming the uncoated RCC and coated RCC emissivity were equal:

$$b \equiv \frac{q_{\text{uncoated}}}{q_{\text{coated}}} = \frac{\sigma(\epsilon T^4)_{\text{uncoated}}}{\sigma(\epsilon T^4)_{\text{coated}}} = \frac{(T^4)_{\text{uncoated}}}{(T^4)_{\text{coated}}} \tag{2}$$

Recent tests have been performed at the JSC arcjet facility in TP2 for uncoated or damaged RCC at higher enthalpies. The Pyrovision infrared camera[‖] was used to obtain a distribution of surface temperatures on one test article as a function of time. In this case, a fully catalytic damage site with exposed carbon substrate was located at the center of the test article (shown in a color temperature contour map in [21]). The results of this test have not yet been published; however, preliminary results have been obtained that indicate a catalytic heating factor of 1.9 based on this temperature distribution and calculations with Eq. (2).[¶] Because of the range of calculated stagnation enthalpies (from 22.1 to 30.2 MJ/kg) and the variation of surface temperature during the tests, it was not possible to obtain a precise value of enthalpy for each catalytic factor. An extreme case of damaged (uncoated) RCC was performed recently at TP2 in which the calculated stagnation enthalpy was about 46.5 MJ/kg, significantly higher than any flight value for orbital return. The range of catalytic heating factors from the evaluation of arcjet data was determined to be 1.62–1.99 [20].

C. Catalytic Recombination Coefficients

To determine the catalytic heating effects analytically, the recombination coefficients for the different surface materials must be defined and modeled correctly. Chemical heating occurs during atmospheric reentry when the temperature of the air becomes large enough to excite and dissociate the air molecules into their respective constituents, namely, oxygen and nitrogen atoms. The catalytic heating depends on the recombination rates of the oxygen and nitrogen atoms of the dissociated air at the wall and their respective heats of formation. If the wall is fully catalytic, all of the atoms in the boundary layer will recombine to become molecules at the wall, releasing the heat of dissociation and increasing the heating rate to the surface. For this case, the flowfield in the vicinity of the surface will essentially be in chemical equilibrium. On the other hand, if the wall is noncatalytic to recombination, none of the atoms recombine to become molecules. In this case, the flow near the surface is essentially frozen at the particular atomic mass concentrations present at the edge of the boundary layer. This produces the lowest heating rate to the surface.

In reality, the surface of the HRSI tiles is neither noncatalytic nor fully catalytic, but partially catalytic. Hence, some of the atoms recombine at the wall, with resulting heating rates ranging between those experienced for a noncatalytic wall and a fully catalytic wall. The glassy outer RCG coating of the Orbiter HRSI tiles tends to have low catalycity compared to metallic surfaces such as copper or columbium which are nearly fully catalytic.

The recombination rates at the wall can be derived from the normal mass flux term in the Navier–Stokes equations for a gas in chemical nonequilibrium [22]. Early analyses [8] used a catalytic recombination speed, k_w, on the order of 700 cm/s for both oxygen and nitrogen recombination at the surface. However, later studies generated separate recombination rates for oxygen and nitrogen recombination based on experimental data. These rates have been determined as a function of wall temperature from data in arcjet facilities for RCG coatings on HRSI tiles [6,23].

General expressions for RCG-coated tile [6] recombination rates have been developed and used in the literature for the predictions of surface heating rates for several years. The oxygen recombination coefficient γ_{O} for two ranges of surface temperature [6] is

$$\gamma_{\text{O}} = 40e^{-11{,}440/T_w} \qquad 1435\ \text{K} < T_w < 1580\ \text{K} \tag{3}$$

$$= 39 \times 10^{-9} e^{21{,}410/T_w} \qquad 1580\ \text{K} < T_w < 1845\ \text{K} \tag{4}$$

The nitrogen recombination rate coefficient γ_{N} for two ranges of surface temperature [6] is

$$\gamma_{\text{N}} = 6.1 \times 10^{-2} e^{-2480/T_w} \qquad 1410\ \text{K} < T_w < 1640\ \text{K} \tag{5}$$

$$= 6.1 \times 10^{-4} e^{5090/T_w} \qquad 1640\ \text{K} < T_w < 1905\ \text{K} \tag{6}$$

Combined, these expressions make up the two-equation temperature-dependent model for the partially catalytic recombination coefficients for HRSI RCG-coated tiles. The two-equation temperature-dependent nitrogen and oxygen recombination coefficients for RCG [6], C742 [7], and RCC (C-CAT) [24], as well as the two-equation temperature-dependent air recombination coefficient model for RCG [24] are plotted vs temperature in Fig. 2a. Although a four-equation model for RCG partially catalytic recombination coefficients is available [24], the two-equation model was used in this analysis for consistency with previous analyses. Analyses with both the four-equation and two-equation models for

[‖]The M9104 Mikron Pyrovision infrared camera (imaging pyrometer) was manufactured by Mikron Infrared, Inc., of Oakland, NJ.

[¶]Information transmitted from A. Rodriguez and R. Lewis/NASA-JSC to W. Rochelle/ESCG-Jacobs, 2005.

RCG recombination coefficients were performed to understand the differences in the two models. An example plot for this comparison is shown in Fig. 2b for a streamline out to the Orbiter wing leading edge. The results of the comparison revealed that the difference between the models is insignificant. The difference is insignificant because the extra two equations in the four-equation temperature-dependent model are for temperatures below 900 K, which is lower than any temperatures observed in the cases studied for catalytic heating.

A large database of temperature-varying recombination rates was generated in arcjets and sidearm reactors at NASA Ames Research Center several years ago [24]. Equations (3–6) as well as other equations in this database have been used in boundary layer programs such as the BLIMPK code [5], and in CFD programs such as the Langley aerothermodynamic upwind relaxation algorithm [25] (LAURA) and the general aerodynamic simulation program (GASP) code [26] to predict heating rates on partially catalytic surfaces.

D. Standard Two-Layer Methodology

The standard two-layer methodology is an inviscid/viscous analysis consisting of an inviscid solution for the freestream flow to the edge of the boundary layer and a viscous boundary layer analytical procedure to calculate the flow properties and heating effects from the edge of the boundary layer to the surface. The boundary layer analysis for this catalytic heating study was conducted with the BLIMPK code [5]. In past analyses with the BLIMPK code, the streamline inputs needed from the inviscid solution were usually extracted from inviscid Euler solutions. In a preliminary analysis, the BLIMPK code was used with the streamline inputs extracted from an existing inviscid Euler solution obtained from the inviscid equilibrium code in three dimensions (IEC3D) [27,28]. The streamlines were extracted along the Orbiter centerline for Mach 12 and 18 in the STS-2 trajectory with the axisymmetric analog two-layer convective heating (AA2LCH) procedure [29]. Figure 3 shows the flight data compared to the BLIMPK analysis for partially catalytic RCG with C742 tiles and for full equilibrium for Mach 18. The forward most catalytic location is magnified in Fig. 3b. Because the preliminary BLIMPK analysis verified the thermochemical model in the BLIMPK code could satisfactorily model the catalytic heating overshoot observed along the centerline in the OEX flight data, NASA-JSC requested that further analyses be conducted to model the catalytic heating effects observed on the Orbiter in the STS-2, -3 and -5 trajectories. However, since inviscid Euler solutions have largely been supplanted by CFD Navier–Stokes solutions, a new method for obtaining the streamline inputs to BLIMPK was needed.

The heating rate ratios in Fig. 3 (and subsequent heating ratio plots) represent the actual heating rates (prediction or flight data) divided by the Fay and Riddell [30] reference heating rate for a 0.3048-m radius sphere at the appropriate trajectory point. This ratio was used because Orbiter flight data is export controlled by the international traffic in arms regulation (ITAR). The error bands in this figure and subsequent figures that show flight data are based on the percent accuracy as listed in the OEX data reports [2–4].

E. Modified Two-Layer Methodology

The catalytic heating analysis presented in this paper was performed with a modified two-layer approach rather than the standard two-layer method. Similar to the standard two-layer approach, the modified two-layer approach consists of the boundary layer solution with the BLIMPK code, but uses extracted streamline inputs from three-dimensional Navier–Stokes (viscous) solutions at the edge of the boundary layer instead of data from inviscid Euler solutions. The streamline inputs are extracted with a streamline mapping algorithm called SRFTRACE [31], described in more detail in the next section. The SRFTRACE algorithm is similar in nature to the AA2LCH procedure used to extract streamline inputs from the inviscid Euler solutions and calculates the same streamline inputs needed for the BLIMPK code including streamline distance, metric coefficient, pressure distribution, and entropy gradient. However, the SRFTRACE code is also capable of extracting the boundary layer edge species mass fractions from chemical nonequilibrium Navier–Stokes solutions, a capability not present in the AA2LCH code. With these streamline inputs, a nonequilibrium, nonisentropic analysis with defined boundary layer edge species mass fractions can be performed with BLIMPK. Thus, in order to perform the catalytic heating analysis with the modified two-layer approach, three analytical tools were used in the following order: the data-parallel line relaxation (DPLR) CFD code [32], the SRFTRACE code, and the BLIMPK code.

1. DPLR

The DPLR CFD code [32] was used to compute laminar Navier–Stokes solutions at discrete trajectory points (time, altitude, and Mach number) for the Orbiter. All of the streamlines considered in the BLIMPK catalytic heating analysis originate from DPLR solutions. DPLR employs a thermochemical model and uses the four-equation temperature-dependent recombination model for RCG [23] for the entire windward acreage. Orbiter grid models exist for low resolution (2.54-cm spacing between grid points) and high resolution (6.35-mm spacing between grid points) computational analyses [33]. It is possible to perform localized catalytic heating analyses for the Orbiter with the DPLR code, but it is time and resource intensive. Because catalytic heating analyses may be needed at discrete points while the Orbiter is in flight, the time needed to complete a localized catalytic heating analysis with DPLR can be restrictive. Additionally, this time requirement precludes the use of DPLR for rapid turnaround, large-scale parametric studies like those

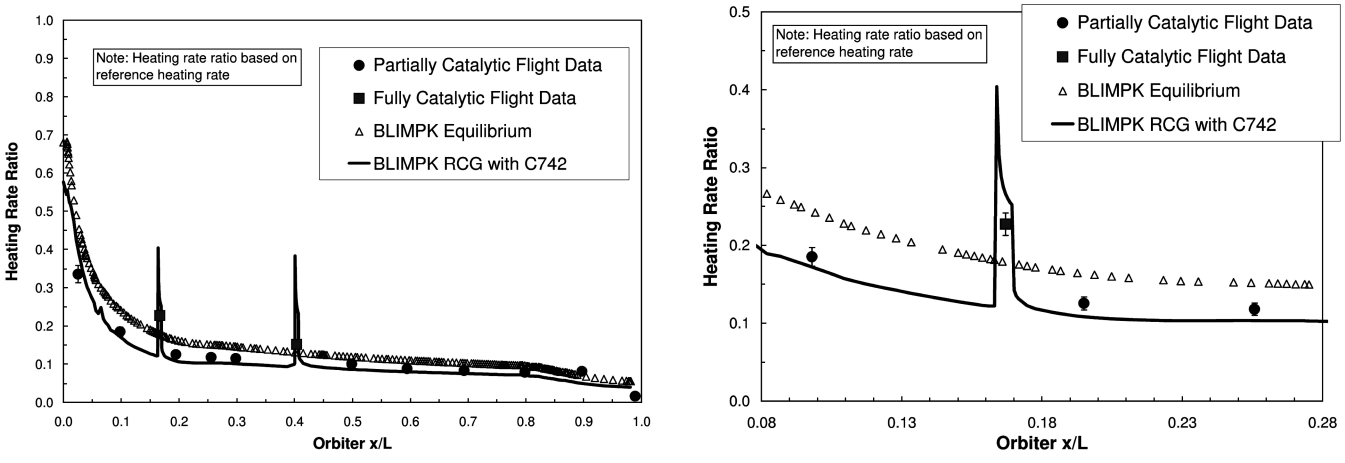

a) Heating rate ratio for Orbiter centerline **b) Magnified**

Fig. 3 Standard BLIMPK/IEC3D two-layer methodology compared to OEX flight data for Mach 18 in the STS-2 trajectory.

considered in the present work. However, DPLR laminar solutions for RCG partially catalytic tiles exist for a number of trajectory points from which streamline inputs can be extracted. All of the DPLR solutions used in this work are for a nominal reentry angle of attack of 40 deg and range between Mach numbers of 6 and 25 for the STS-107 trajectory [34]. The simulations employed a 5-species chemical nonequilibrium, thermal equilibrium model. DPLR-calculated heating rates are compared with the BLIMPK-calculated heating rates in Sec. III. All of the streamline inputs for BLIMPK were extracted from the DPLR Navier–Stokes solutions with the SRFTRACE code.

2. SRFTRACE

The SRFTRACE code was used to map the data needed from the three-dimensional Navier–Stokes simulations into the format required for the BLIMPK code. The principal data inputs required for BLIMPK are the boundary layer edge properties, the spatial location of the surface points, and the streamline metric coefficient. These first two input sets are trivially obtained from the CFD volume solutions, but the computation of the streamline metric coefficient warrants further explanation.

Figure 4 shows a representative streamline on the lower surface of the Orbiter. The reference coordinate system is denoted by the (x, y, z) axes, which is the coordinate system used in the CFD solver. The (ξ, η, ζ) streamline coordinate system is introduced to provide the mapping for BLIMPK. In this curvilinear coordinate system the ξ axis is tangential to the streamline and the ζ axis is normal to the surface of the vehicle. The η axis is normal to the streamline on the surface of the vehicle and completes the system.

An arbitrary location can be expressed in the reference Cartesian coordinates as

$$r = x\hat{i} + y\hat{j} + z\hat{k} \tag{7}$$

Furthermore, points on the surface of the vehicle can also be defined as

$$r = \xi\hat{e}_\xi + \eta\hat{e}_\eta \tag{8}$$

The unit vector $\hat{e}_\eta$ may be expressed as

$$\left|\frac{\partial r}{\partial \eta}\right|\hat{e}_\eta = \frac{\partial r}{\partial \eta} \tag{9}$$

where the magnitude term on the left-hand side of the equation denotes the metric coefficient required by BLIMPK. This quantity measures the effective radius of curvature of the vehicle surface in the direction normal to the streamline.

Consider the identity

$$\frac{\partial}{\partial t}\left(\frac{\partial r}{\partial \eta}\right) = \frac{\partial}{\partial t}\left[\frac{\partial x}{\partial \eta}\hat{i} + \frac{\partial y}{\partial \eta}\hat{j} + \frac{\partial z}{\partial \eta}\hat{k}\right] \tag{10}$$

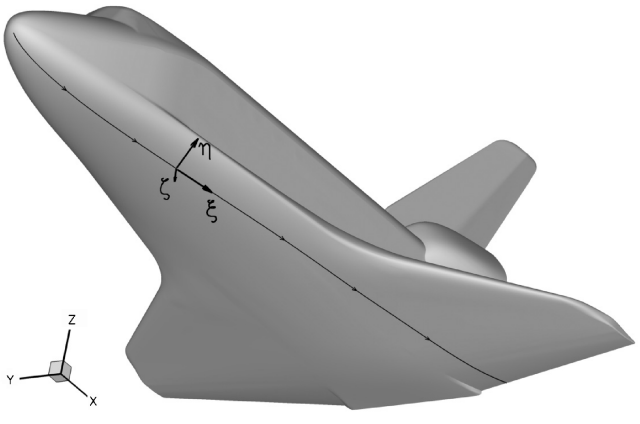

Fig. 4 Reference and streamline coordinate systems.

which, upon rearranging the order of differentiation in the right-hand-side, becomes

$$\frac{\partial}{\partial t}\left(\frac{\partial x}{\partial \eta}\right) = \frac{\partial}{\partial \eta}\left[\frac{\partial x}{\partial t}\hat{i} + \frac{\partial y}{\partial t}\hat{j} + \frac{\partial z}{\partial t}\hat{k}\right] = \frac{\partial}{\partial \eta}[u\hat{i} + v\hat{j} + w\hat{k}] = \frac{\partial V}{\partial \eta} \tag{11}$$

The last term on the right-hand side may be expanded using the following identity:

$$\frac{\partial(\,)}{\partial \eta} \equiv \frac{\partial x}{\partial \eta}\frac{\partial(\,)}{\partial x} + \frac{\partial y}{\partial \eta}\frac{\partial(\,)}{\partial y} + \frac{\partial z}{\partial \eta}\frac{\partial(\,)}{\partial z} \tag{12}$$

Using (12) in (11) yields the following system of ordinary differential equations:

$$\frac{\partial}{\partial t}\left(\frac{\partial r}{\partial \eta}\right) = \frac{\partial r}{\partial \eta}\cdot\nabla V \tag{13}$$

which defines an initial-value problem for the metric coefficient distribution along a given streamline. At the stagnation point of the vehicle the nose radius is known and defines the initial value of the metric coefficient. An explicit time integration technique is used to compute the metric coefficient at downstream locations, similar to the approach outlined in [32].

This procedure is implemented in a C++ code called SRFTRACE. This tool uses the libMesh[**] open-source finite element library to read the surface and boundary layer edge parameters, along with the surface grid. The surface grid is treated as a hybrid-element unstructured mesh, which removes any constraints on the topology of the original grid. The standard piecewise linear Lagrange basis functions are used for interpolation along the surface. The boundary layer thickness and edge properties are located using the curvature method described in [35].

The user specifies a point of interest on the surface, and a streamline is generated via explicit integration in the direction opposite of the boundary layer edge velocity. This procedure terminates in the upstream direction when the stagnation point is located. The streamline may also be extended downstream of some user-specified distance if desired. The resolution of the points along streamlines depends on the resolution of the Navier–Stokes solution. In this study, the highest-resolution grids currently available for Orbiter RTF reentry [33] simulations were used, providing a streamwise point distribution on the order of 6.35 mm. At each point along the streamline the tool interpolates a number of values from the CFD data including 1) surface pressure, 2) species mass fractions at the edge of the boundary layer, 3) total energy, and 4) boundary layer edge velocity. The velocity gradient is also computed, as is the entropy and surface normal. In the current implementation, the entropy is computed assuming local equilibrium using the curve fits by Tannehill [36]. It would be preferable to interpolate the entropy directly from the CFD solutions as well, but this is not supported with the existing postprocessing tools. The tool outputs a table including all the information needed by BLIMPK, and optionally can produce a Tecplot®[††] binary surface file including all the derived parameters for inspection.

3. BLIMPK

The bulk of the catalytic heating analysis, including calculation of the catalytic heating factors, was performed with the BLIMPK code, a FORTRAN based code developed by Aerotherm for NASA for use in aeroheating analyses during the Apollo program. The BLIMPK code was used in this analysis to calculate localized catalytic heating at points along centerline streamlines and streamlines out to the wing tile acreage and wing leading edge. The BLIMPK model, described in the latest User's Guide [5], incorporates temperature-dependent catalytic models and uses a maximum of 15 nodes across the

[**]Data available on-line at http://libmesh.sourceforge.net [cited 9 February 2005].

[††]Data available on-line at http://www.tecplot.com [6 March 2005].

Table 1 Freestream and stagnation properties for STS-5 and STS-107 best-estimate trajectories

Flight	Time From EI, s	Altitude, km	Mach no.	Stagnation enthalpy, MJ/kg	Stagnation pressure, Pa
STS-5	810.0	63.569	18	16.017	5,511.5
STS-107	375.8	75.722	25	27.538	1,981.5
STS-107	602.4	70.381	23	24.014	3,482.3
STS-107	916.3	62.124	18	15.887	5,132.5
STS-107	993.1	58.818	16	13.070	8,345.2
STS-107	1339.6	39.850	6	2.363	14,416.6

boundary layer. Subsequent modifications allow the catalytic model to be updated at each station along the streamline, as well as the ability to model up to 2500 streamline stations. Macros and scripts have been used to speed up the preprocessing of the BLIMPK input files for large parametric studies.

The BLIMPK code input was set up to model a chemically nonequilibrium boundary layer of five species with finite gas reaction rates for nonisentropic flow around a body. The inputs also included streamline distance, metric coefficient, pressure distribution, boundary layer edge species mass fractions, and entropy gradient. In addition, BLIMPK required stagnation enthalpy and pressure values which were extracted from the best-estimated trajectory for STS-5 [4] and STS-107 [34], the two trajectories used in this analysis. These stagnation values are provided in Table 1.

F. Orbiter Locations Investigated

One of the goals of this analysis was to determine how well nonequilibrium, nonisentropic BLIMPK results based on the modified two-layer methodology would match the STS-2, -3, and -5 OEX flight data. Because the STS-5 mission had six near-centerline C742 catalytic tiles in addition to the two wing C742 catalytic tiles, the STS-5 best-estimate trajectory was used for a major part of the present analysis. To verify that the BLIMPK analysis was suitable for predicting the catalytic overshoot phenomena encountered during Orbiter atmospheric reentry, all of the centerline C742 catalytic sensors were investigated, as well as the two C742 coated wing tiles on STS-5. The thermocouple locations for the centerline sensors and two wing sensors on the Orbiter used for this analysis are listed in Table 2 [2–4]. Validating the current approach with these flight data allowed the methodology to be applied to the Orbiter nose cap, lower fuselage acreage, wing acreage, and wing leading edge with confidence.

The STS-5 BLIMPK wing analysis was compared to the STS-5 C742 highly catalytic flight data measurements mainly to judge the ability of the modified two-layer methodology to predict catalytic heating jumps on streamlines out to locations on the Orbiter wing. The two streamlines to the catalytic tile locations on the underside of the left wing on STS-5 pass very close to the bow shock/wing shock interaction region (called the shock–shock region, or SSI) on the wing leading edge (in the vicinity of RCC panels 8 and 9), as shown in Fig. 5. In past analyses, there have been problems running BLIMPK with the adverse pressure gradient that occurs in the SSI region [37]. This current analysis proves that BLIMPK can handle the large adverse pressure gradients which occur along the streamline near the shock–shock interaction region on the wing leading edge, provided that the appropriate boundary layer edge properties are used. One observation from the current analysis is that it is critical to account for entropy swallowing in the presence of adverse pressure gradients when using this modified two-layer methodology.

The other purpose of this document is to present the predictions of the BLIMPK surface catalytic heating analyses for fully catalytic repair/damage locations at specific RCC sites including the nose, chin panel, and wing leading edge. The present BLIMPK surface catalytic heating analysis was performed for two RCC nose cap body point locations, one on the windward side and one on the leeward side, and one chin panel location slightly below the nose cap. Streamlines for three panels with six zones per panel for the STS-107 trajectory were investigated, each passing through a respective body point on the wing leading edge of the Orbiter. A schematic of the wing leading edge panel showing the zone locations is shown in Fig. 6a [38]. The definition of these zones was developed by the Orbiter LESS/RCC PRT for use in damage assessment.

Table 2 STS-5 data sensor locations

Sensor label	*Xo*, m	*Yo*, m	*Zo*, m
V09T9341A	6.800	0.000	7.775
V07T9452A[a]	9.182	−0.132	7.254
V07T9463A[a]	11.440	0.000	7.076
V07T9464A[a]	12.357	−0.163	7.046
V09T9381A	14.351	−0.109	7.000
V07T9468A[a]	15.751	0.000	6.970
V07T9471A[a]	19.200	0.000	6.894
V09T9521A	22.324	−0.325	6.828
V07T9478A[a]	25.451	0.000	6.756
V07T9481A	28.684	0.000	6.685
V07T9487A	32.131	0.000	6.609
V07T9489A	35.367	0.000	6.675
V07T9492A	38.387	0.000	6.980
V07T9689A[b]	31.054	7.120	7.211
V07T9692A[b]	32.870	7.059	7.163

[a]C742 coated tile.
[b]C742 coated wing tile.

Table 3 contains the body point locations on the nose, chin panel, and wing leading edge for the RCC catalytic heating analysis [39]. The body points for panels 7 and 9 in Table 3 are taken along a normal cut to wing leading edge. Figure 6b shows the panel 9 normal cuts in detail with the body point locations labeled. The body points for panel 11 are taken along a planar cut in the *X* direction at constant value of *Y* at 60% semispan [39].

The RTF BLIMPK analysis for these cases was performed to determine local fully catalytic heating bump factors at different locations on the Orbiter RCC nose, chin panel, and wing leading edge for specific times (Mach numbers) in the STS-107 trajectory. The BLIMPK-predicted catalytic factors for the RCC critical regions were calculated for comparison to the original catalytic factors derived from the OEX flight data sensors for the STS-2, -3, and -5 C742 highly catalytic tiles [11].

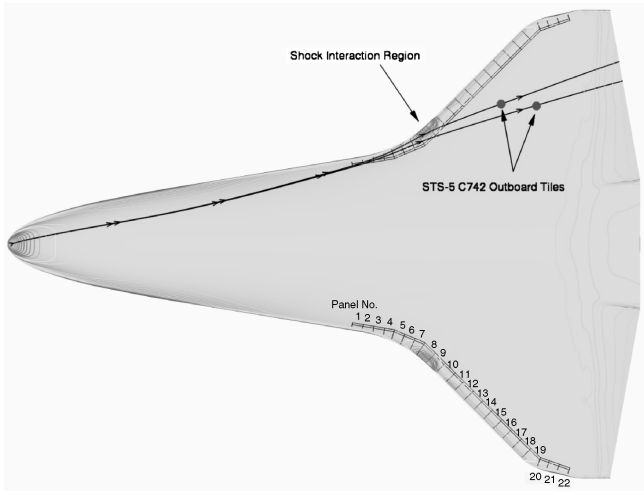

Fig. 5 Surface pressure contours and streamlines to wing C742 tiles. RCC panel locations shown for reference.

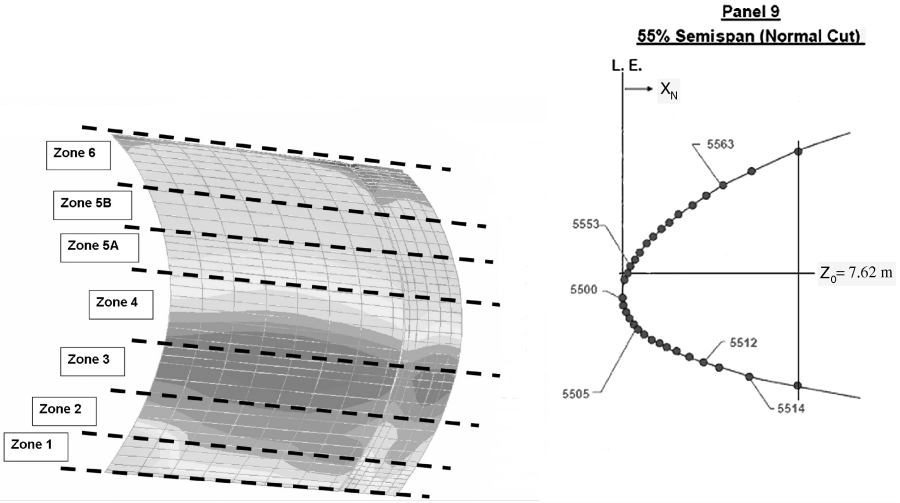

a) Schematic of wing leading edge panel showing zone locations with color-shaded surface temperature mapping from a Boeing 3D Thermal Math Model solution [38]

b) Schematic of panel 9 showing normal cut on RCC wing leading edge and body point locations [39]

Fig. 6 RCC panel geometry and body point locations.

G. Assumptions and Cases Analyzed

Several defining assumptions were made to perform the BLIMPK catalytic surface heating analysis. These assumptions are listed below:

1) Nonequilibrium, nonisentropic (Tannehill equilibrium entropy curve fits [36]) solution with species mass fractions defined at the boundary layer edge (five species models: N, O, NO, N_2, O_2).

2) NASA Ames Research Center two-equation temperature-dependent models for RCG, C742, and C-CAT (RCC) recombination coefficients from [6,7,24], respectively.

3) Temperature-dependent RCG emissivity used for the entire analysis [7].

4) C742 catalytic recombination coefficients for each catalytic tile location (approximately 20.3 cm long) on STS-5 windward tile acreage analysis and fully catalytic recombination coefficients for each repair/damage location (approximately 15.2 cm long for nose and chin panel and 20.3 cm long for wing leading edge) for RCC analysis.

5) Streamline cases for STS-5 trajectory at Mach 18 for the C742 highly catalytic tile locations (listed in Table 2).

Table 3 Body point locations [39]. Note: n/A denotes a nose cap body point location

Panel	Zone	Body point	*Xo*, m	*Yo*, m	*Zo*, m
n/A	n/A	114	6.484	0.000	7.932
n/A	n/A	1000	5.994	0.000	8.598
n/A	n/A	1020	6.785	0.000	7.874
7	1	5115	27.115	5.070	7.130
7	2	5113	26.906	5.331	7.231
7	3	5105	26.731	5.550	7.361
7	4	5100	26.700	5.591	7.463
7	5A	5155	26.731	5.550	7.635
7	6	5163	26.906	5.331	7.945
9	1	5514	28.082	6.261	7.244
9	2	5512	27.976	6.365	7.290
9	3	5505	27.813	6.515	7.414
9	4	5500	27.777	6.543	7.480
9	5A	5553	27.795	6.513	7.635
9	6	5563	28.011	6.271	7.912
11	1	2609	29.200	7.137	7.358
11	2	2607	29.055	7.137	7.379
11	3	2602	28.600	7.137	7.379
11	4	2600	28.372	7.138	7.535
11	5A	4602	28.600	7.137	7.800
11	6	4607	29.055	7.137	8.001

6) Streamline cases for STS-107 trajectory at Mach numbers 25, 23, 18, 16, and 6 for body point locations in six zones at panels 7, 9, and 11 (90 total cases)

The STS-2, -3, and -5 OEX flight data sensor locations are shown in Table 2, the body point locations for the STS-107 analyses are listed in Table 3, and the relevant stagnation properties for each trajectory point investigated are shown in Table 1. All damage/repair sites for the RCC analysis are assumed to be smooth regions with a fully catalytic surface. No cavity damage or repair protuberance effects were assessed in conjunction with the change in surface catalysis. Catalytic location length and recombination coefficient variance sensitivity studies were conducted for selected cases.

III. Results

The following section presents the results of the BLIMPK catalytic heating analysis performed on streamlines for selected points in the STS-5 (for comparison to the OEX flight data) and STS-107 trajectories. All of the heating rate results are presented in nondimensional form as heating rate ratios based on a reference heating rate. The catalytic heating (bump) factors are derived in the same manner as they are in [20], as the local fully catalytic heating rate divided by the partially (nominal) catalytic heating rate at the same location. The centerline, nose cap, and chin panel streamline analyses are evaluated first, and then the wing acreage and wing leading edge streamline analyses are evaluated.

A. Lower Fuselage Centerline Region

The catalytic heating effects from the six C742-coated tiles on the Orbiter windward centerline during the STS-5 mission were evaluated to verify that the BLIMPK code could model the catalytic heating overshoot observed on the STS-5 OEX flight data. Figures 7a and 7b show a Mach 18 comparison of the STS-5 OEX flight data and the BLIMPK-calculated heating rate ratios for the centerline partially catalytic RCG tiles with highly catalytic C742 coating at sensor locations indicated in Table 2. Also shown in Figs. 7a and 7b are the DPLR solutions for the partially catalytic RCG coating.

The entire streamline calculation and all the available centerline flight data are presented in Fig. 7a, and a magnification of the upstream C742 tile locations is shown in Fig. 7b. The flight data for the C742 catalytic locations are for the center of the 20.3-cm tile, where the BLIMPK catalytic heating has dropped significantly from the peak value at the upstream edge of the C742-coated tile. It is at this center location of each BLIMPK catalytic jump that the comparison with the STS-5 OEX flight data was made.

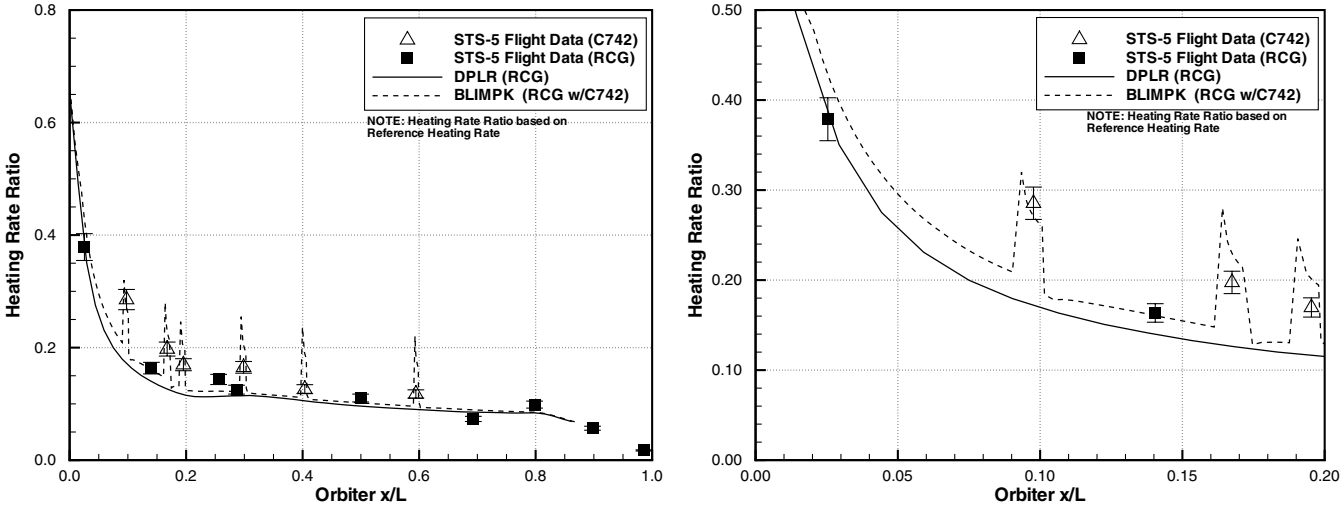

a) Heating rate ratio for Orbiter centerline

b) Magnification

Fig. 7 DPLR and BLIMPK centerline analysis compared to STS-5 flight data for Mach 18.

Figures 7a and 7b show that the BLIMPK-calculated heating rates compare very well with the STS-5 OEX flight data for the RCG and C742 coated tiles. The catalytic heating calculated by BLIMPK at the first C742 tile location slightly underpredicts the STS-5 data value at that location (although it is well within the uncertainty of the data for this location at this point in the trajectory, 6.3% [4]), but the rest of the downstream BLIMPK catalytic heating jumps overshoot the STS-5 flight data. The BLIMPK overshoot for the downstream catalytic locations is expected because BLIMPK does not model the transient properties of the chemical heating occurring during reentry nor does it account for upstream influences. As the dissociated atoms travel downstream, they are partially exhausted by each highly catalytic tile location. Therefore, there are fewer atoms to recombine downstream at the other highly catalytic locations. Because there is more than one localized highly catalytic location along the centerline, this effect can be observed in the STS-5 flight data.

B. Nose Cap/Chin Panel Region

A BLIMPK catalytic heating analysis was performed along centerline streamlines for the STS-107 trajectory to predict catalytic heating effects on the nose cap and chin panel RCC region [20]. To date, there are no flight data with surface catalysis changes in the nose cap/chin panel region with which to compare the BLIMPK results. The analysis was done for leeward and windward streamlines, and both C-CAT (RCC) and RCG partially catalytic models were used to investigate fully catalytic repair/damage sites at body point 114 on the windward side of the nose cap, body point 1000 on the leeward side of the nose cap, and body point 1020 on the chin panel (cf. Table 3).

Figure 8 shows the Mach 18 BLIMPK heating rate ratio results of the windward streamline analysis with the DPLR predicted heating rate ratios included for comparison. The first jump corresponds to BP 114 on the nose cap and the second corresponds to BP 1020 on the chin panel. The DPLR and BLIMPK-calculated heating rate ratios compare very well for both the C-CAT and RCG analyses, but at the stagnation point, the BLIMPK C-CAT (RCC) result compares better with the DPLR result than the BLIMPK RCG result. The C-CAT analysis shows larger catalytic heating overshoots than the RCG analysis because more atomic species (available for recombination) are upstream of the fully catalytic location. This is due to the lower recombination coefficients for C-CAT at the higher temperatures (see Fig. 2a). The catalytic factors for the C-CAT analysis are also larger than the factors for the RCG analysis because the C-CAT partially catalytic heating rates are lower than the RCG partially catalytic heating rates. The BLIMPK C-CAT partially catalytic heating rate increases abruptly after the second fully catalytic jump because of the transition to the RCG HRSI tiles.

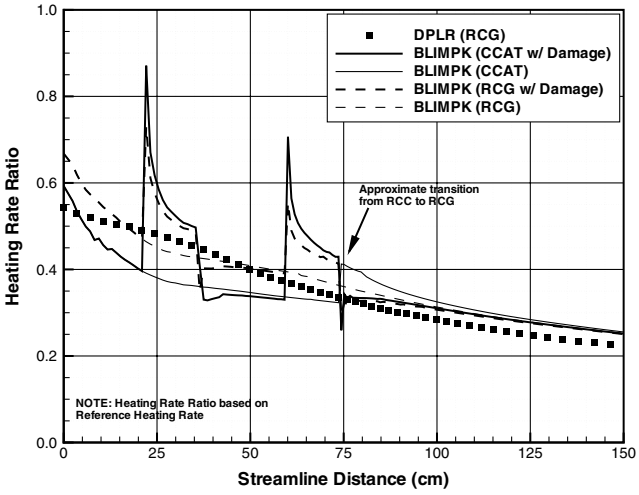

Fig. 8 DPLR and BLIMPK windward centerline analysis for Mach 18 in the STS-107 trajectory.

The two fully catalytic jumps shown in Fig. 8 were examined more closely in the Mach 25 windward centerline analysis. The convective heating rate (represented by the heating rate ratios presented in this paper) transferred to the surface, q_{conv} is the sum of a conduction term, q_{cond} and a chemical term, q_{chem}:

$$q_{\text{conv}} = q_{\text{cond}} + q_{\text{chem}} \tag{14}$$

The convective heating rate contributions from the conductive and chemical heating rate terms are shown in Fig. 9 for the BLIMPK Mach 25 windward centerline analysis. The conductive heating rate is the product of the thermal conductivity of the material and the temperature gradient at the surface. The chemical heating rate is computed from a combination of unequal thermal and multicomponent diffusion coefficients and species concentration gradients [22]. If thermal diffusion is neglected, Eq. (14) can be rewritten as

$$q_{\text{conv}} = -\lambda\left(\frac{\partial T}{\partial \zeta}\right) + \sum_i \beta_i h_i^0 M_i \tag{15}$$

where the normal mass flux of the ith species, M_i, may be expressed as

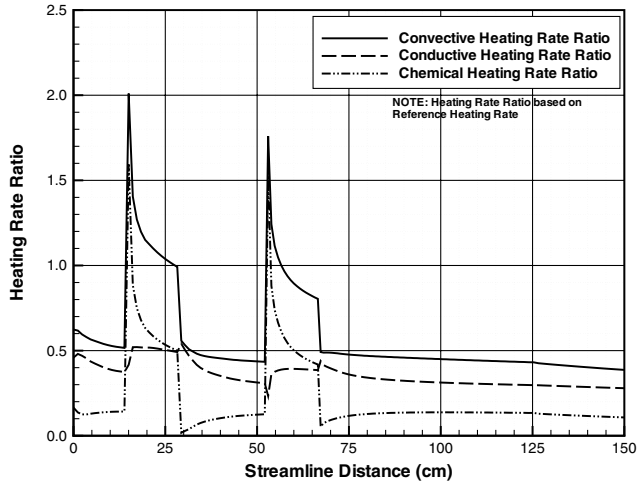

Fig. 9 BLIMPK Mach 25 windward centerline heating rate components.

$$M_i = \rho \sum_j D_{ij} \left(\frac{\partial C_j}{\partial \zeta} \right) \tag{16}$$

where the summation is over all species.

In Eq. (15), the chemical energy accommodation coefficient β is assumed to be equal to 1.0. This implies that all of the chemical energy created by surface recombination goes into the chemical surface heating of the vehicle.

The chemical (or catalytic) heating occurs during hypersonic reentry and causes increased heating at the surface of the Orbiter. The air molecules (mostly molecular nitrogen and oxygen, or N_2 and O_2) are highly excited by the hypersonic shock wave and dissociate into their atomic constituents, N and O, which may then react to form nitric oxide, NO. At the surface, the atoms may recombine to form molecules, releasing their dissociation energy in the form of heat which is then transferred into the surface. The rate of recombination determines the amount of chemical, or catalytic, heating. Some surfaces are very prone to massive recombination (highly catalytic materials), whereas some are deterrents to recombination (partially catalytic materials). By tracking the species mass fraction concentrations, the level of recombination, or catalycity, can be observed.

Figure 10 exhibits the five species mass fraction concentrations on the Orbiter windward centerline at Mach 25 in the STS-107 trajectory. Between 0.0 and 15.2 cm and 30.5 and 51.8 cm, C-CAT recombination coefficients are being used for the surface heating calculations. In these areas, the species mass fraction concentrations appear nominal for hypersonic reentry. Oxygen is almost fully dissociated, shown by the high amount of oxygen atoms compared to the number of oxygen molecules. There are more nitrogen molecules than nitrogen atoms in the partially catalytic region because nitrogen has a higher excitation temperature and, therefore, does not dissociate as quickly as oxygen. At the fully catalytic damage sites, between 15.2 and 30.5 cm and 51.8 and 67.1 cm, there are significant increases in the N_2, O_2, and NO molecules, while there are also significant decreases in the amount of atomic nitrogen and oxygen. The increase in nitrogen and oxygen molecules shows that much more recombination is occurring, hence the higher heating rates seen in Fig. 9. After 67.1 cm, the species mass fraction concentrations appear nominal once again, but are now higher than they were for the other partially catalytic regions because the RCG recombination coefficients were used for the surface heating calculations at this point.

The BLIMPK catalytic heating analysis along centerline streamlines for the STS-107 trajectory was performed to obtain catalytic heating factors on the critical nose cap and chin panel RCC region to be used in real-time thermal analyses for future shuttle flights [20]. Catalytic heating factors were calculated for fully catalytic repair/damage on the nose cap and chin panel region with RCG and C-CAT (RCC) partially catalytic heating rates at the trajectory points listed in Table 1 for STS-107. The RCG and C-CAT derived midpoint catalytic heating factors obtained from this analysis are plotted in Fig. 11 along with the recommended catalytic model for the orbiter nose region proposed in April 2004 (based on the OEX flight data analysis in [11]) and in March 2005 as an upper limit (based on the STS-107 analysis with BLIMPK). Arcjet test data points (described earlier) are also shown for comparison. As mentioned before, the catalytic factors predicted by BLIMPK based on the C-CAT partially catalytic heating rates are higher than the factors based on the RCG partially catalytic heating rates. In general, the catalytic factors obtained on the leeward side of the nose cap (where partially catalytic heating rates are lower) tend to be more severe than the catalytic factors obtained for the windward side. The catalytic factors also tend to decrease with decreasing stagnation enthalpy and as the damage location moves further away from the stagnation point.

C. Wing Acreage Region

A major focus of this BLIMPK catalytic surface heating analysis was the Orbiter wing tile acreage for STS-5. One of the major objectives of this analysis was to prove BLIMPK could successfully handle the large adverse pressure gradient induced by the Orbiter bow and wing leading edge (WLE) shock–shock interaction and determine how well BLIMPK could model the catalytic heating overshoot observed in the flight data on the two C742 highly catalytic

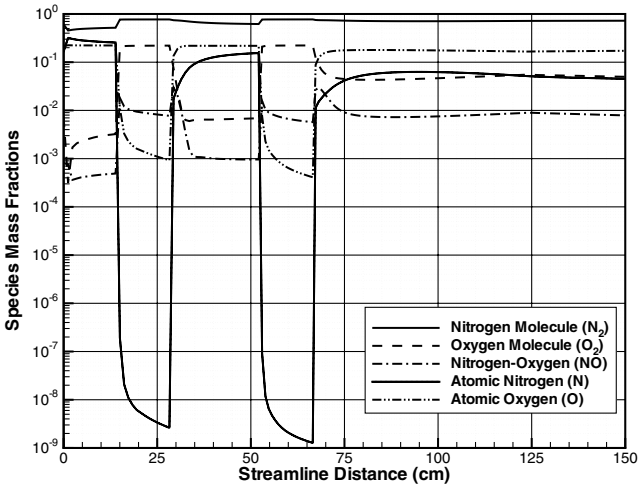

Fig. 10 BLIMPK Mach 25 windward centerline species mass fractions.

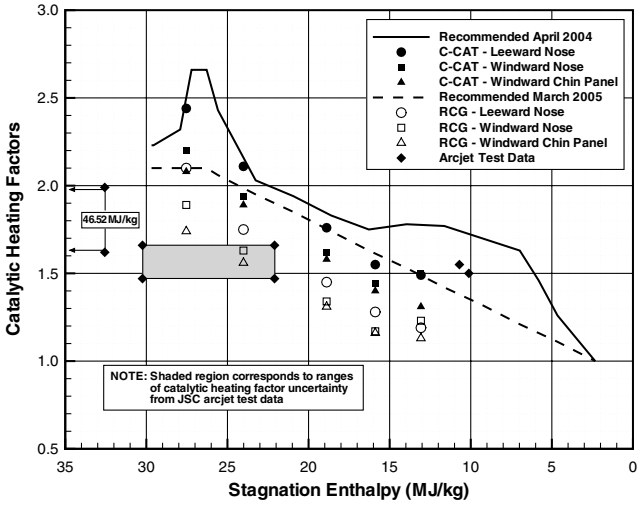

Fig. 11 Midpoint catalytic factors derived from Orbiter centerline RCC nose cap analysis.

wing acreage tiles [40]. Streamlines passing through these sensors are shown in Fig. 5.

The convective heating rate ratio results for the Mach 18 streamline out to the V07T9689A sensor on the Orbiter during STS-5 are shown in Fig. 12a with the C742 catalytic jump at a streamline distance of approximately 26 m. Both the DPLR solution heating rates and the BLIMPK solution heating rates are shown for comparison. STS-2 and -3 had very similar RCG partially catalytic heating rates at the sensor location, but only the heating rate at the sensor location for STS-3 is shown. The DPLR and BLIMPK generated heating rates are very close, and the BLIMPK solution was able produce the same peak heating rate in the adverse pressure gradient near the SSI region. Figure 12b shows the magnification of the V07T9689A sensor location along the STS-5 M 18 streamline. The DPLR heating rate ratio at the sensor location is slightly lower than the STS-3 partially catalytic heating rate ratio, while the BLIMPK partially catalytic heating rate ratio is even lower. The BLIMPK-predicted value at the center of the C742 tile (location of the flight data measurement) comes very close to the STS-5 flight data value and is only slightly lower when uncertainty is included (6.3% [4]). The BLIMPK prediction could possibly be higher if more data points were included across the tile.

The convective heating rate ratio results for the Mach 18 streamline out to the V07T9692A sensor on the Orbiter during STS-5 are shown in Fig. 13a with the C742 catalytic jump at a streamline distance of approximately 27.4 m. Both the DPLR solution heating rates and the BLIMPK solution heating rates are shown for comparison. Again, although STS-2 and -3 had very similar RCG partially catalytic heating rates at the sensor location, only the heating rate at the sensor location for STS-3 is shown. The DPLR and BLIMPK generated heating rates are very close, but there is a larger difference between the peak heating rates in the two solutions at the adverse pressure gradient near the SSI region. Figure 13b shows the magnification of the V07T9692A sensor location. The DPLR heating rate at the sensor location is in close agreement with the STS-3 partially catalytic heating rate, while the BLIMPK partially catalytic heating rate is even closer. The BLIMPK-predicted value at the center of the C742 tile is greater than the STS-5 flight data value even with the uncertainty of the flight data measurement (6.8% [4]).

Although the BLIMPK heating rate value for the V07T9689A sensor streamline is slightly lower than the flight data measurement at the sensor location, the BLIMPK derived highly catalytic to partially catalytic heating rate bump factor is higher. The BLIMPK-calculated bump factor (1.39) is slightly higher than the factor computed from the STS-5 highly catalytic heating rate and the STS-3 partially catalytic heating rate (1.33) for the V07T9689A sensor location. The BLIMPK highly catalytic to partially catalytic heating rate bump factor for the V07T9692A sensor location is also slightly higher

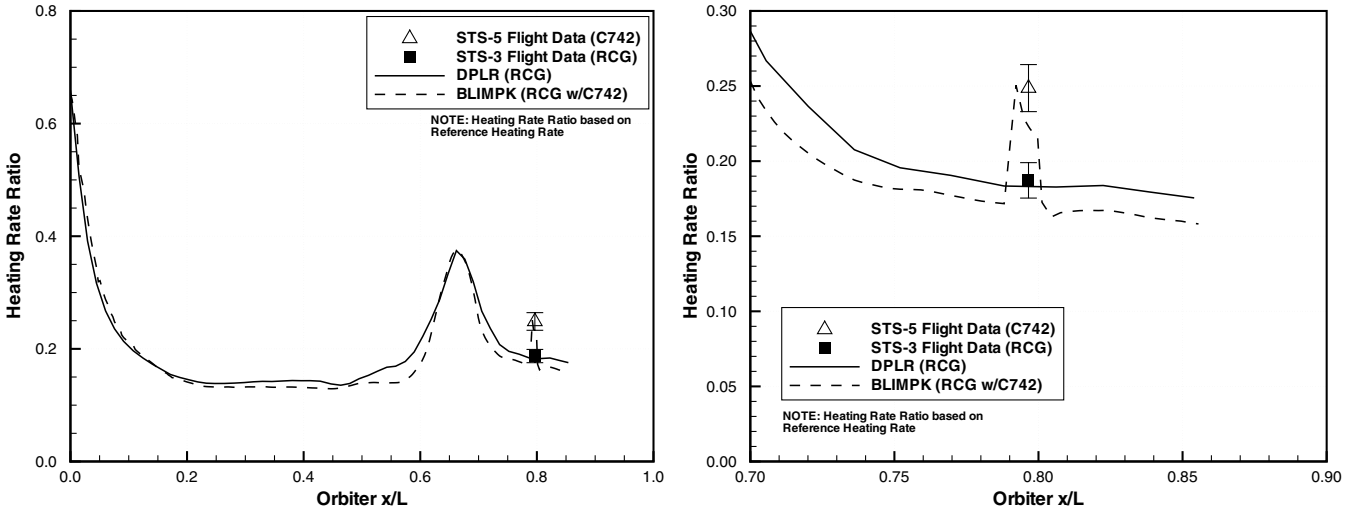

a) Heating rate ratio for entire streamline **b) Magnification**

Fig. 12 DPLR and BLIMPK-predicted heating rates for OEX sensor location V07T9689A on the Orbiter wing at Mach 18 in the STS-5 trajectory.

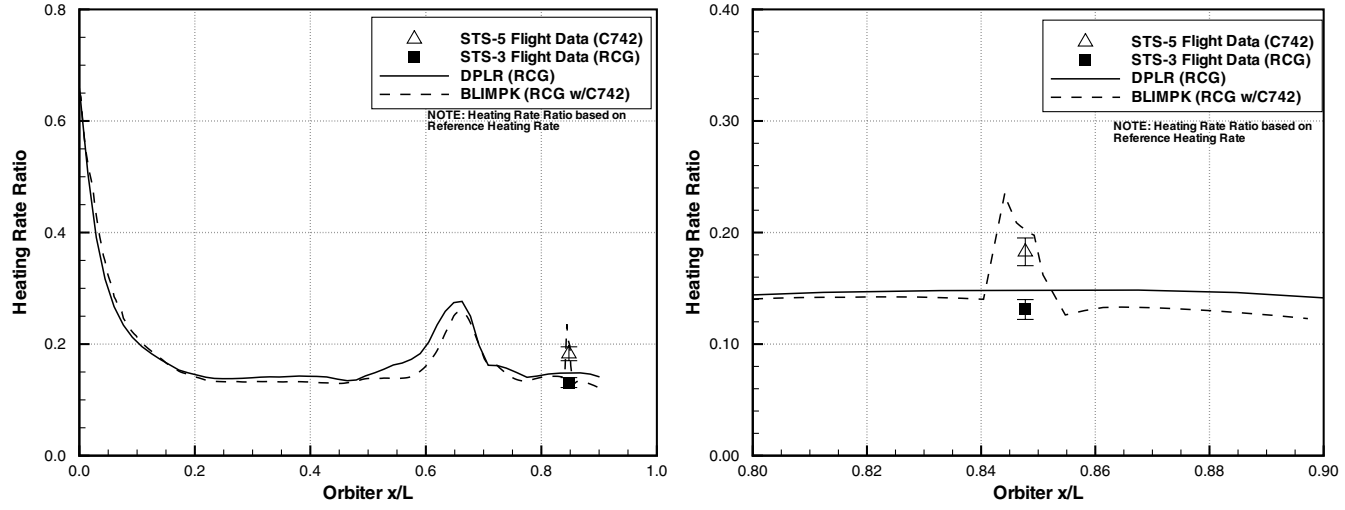

a) Heating rate ratio for entire streamline **b) Magnification**

Fig. 13 DPLR and BLIMPK-predicted heating rates for OEX sensor location V07T9692A on the Orbiter wing at Mach 18 in the STS-5 trajectory.

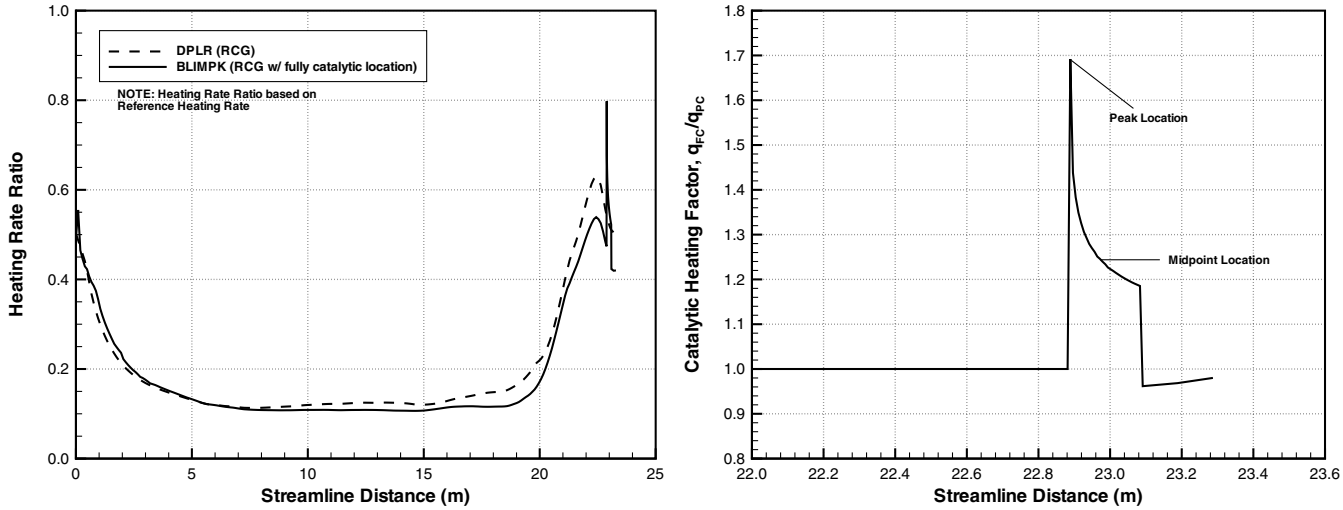

a) Heating rate ratio for entire wing streamline **b) Magnification**

Fig. 14 DPLR and BLIMPK results for the fully catalytic region at Orbiter RCC panel 9, zone 3 at Mach 23 in the STS-107 trajectory.

(1.47) than the value computed from the STS-5 highly catalytic heating rate and the STS-3 partially catalytic heating rate (1.4).

D. Wing Leading Edge Region

The purpose of the BLIMPK analysis [40] along the off-centerline (wing) streamlines was to obtain catalytic heating factors for certain STS-107 trajectory points at locations on the RCC wing leading edge which could be applied in a thermal math model. The catalytic heating factors obtained from the new analysis would supplement the factors for the wing presented in [11]. Although 90 streamline cases were analyzed, the BLIMPK code was able to achieve converged solutions for only 85 of those cases. All streamlines for panel 7, zone 6 were unable to reach convergence, possibly due to the very deep expansion around the wing leading edge that occurs at that location.

Of the 85 converged solutions, the worst case heating rates and temperatures occur during Mach 23 in the STS-107 trajectory in the shock–shock interaction region on the wing leading edge at panel 9, zone 3. Figure 14a shows the worst case heating to the RCC wing leading edge at panel 9, zone 3 for Mach 23 in the STS-107 trajectory. The 20.3-cm fully catalytic damage location is shown at a streamline distance of approximately 22.86 m. The BLIMPK-predicted heating rate ratios are very close to those predicted by the DPLR CFD solution up until a distance of about 6.1 m at which point the two solutions diverge to a maximum difference at the peak heating location on the RCC wing leading edge. The maximum difference in the heating between the BLIMPK and DPLR solutions occurs at the higher Mach numbers (the worst case is Mach 25). The difference drops as the Mach number (or enthalpy) decreases. This difference may be because the current BLIMPK analysis assumes local equilibrium when computing the entropy gradient along the streamline as discussed previously. This approach should be most accurate near the stagnation point of the vehicle where the boundary layer edge Mach number is low and would become increasingly invalid as the flow accelerates rapidly around the vehicle, violating the assumption of local equilibrium.

Figure 14b shows a magnification of the fully catalytic damage site bump factor where the asymptotic peak and the exponential decay of the catalytic overshoot can be seen over the entire catalytic location. The peak catalytic factors and the catalytic factors at the midpoint were obtained for each converged solution and are presented in [40]. The real in-flight catalytic heating factor at the leading edge of the damage location is in between these two values. Although the worst case heating rates and temperatures occur on panel 9, zone 3 (windward), the worst case catalytic factors actually occur on the leeward zones (zones 5A and 6).

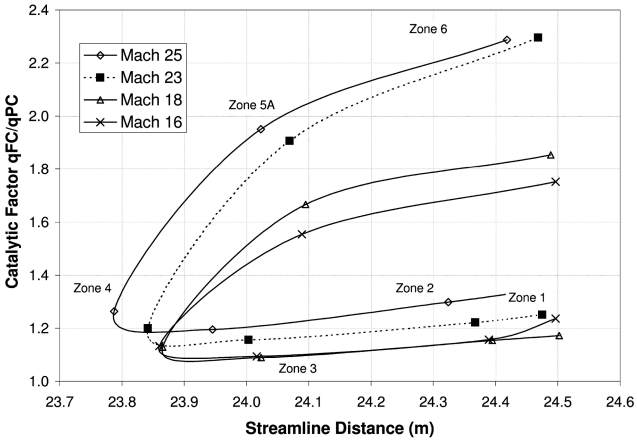

Fig. 15 Midpoint catalytic factors for panel 11.

Figure 15 displays the midpoint catalytic bump factors versus streamline distance in meters for all zones (for converged solutions) for panel 11. The figure shows that zones 3 and 4 are closer to the apex of the wing leading edge and have the lowest catalytic factors, whereas the more windward and leeward zones have higher catalytic factors with the highest bump factor at either zone 5A or 6. The peak and midpoint catalytic bump factors for all converged cases along with the location and trajectory information and the fully catalytic and partially catalytic heating rates are contained in [40]. The Mach 6 cases were not evaluated as extensively as all fully catalytic bump factors were calculated to be unity, consistent with the negligible dissociation levels for this low freestream enthalpy (approximately 2.326 MJ/kg, cf. Table 1).

In Fig. 16, the recommended catalytic heating factor model for the Orbiter wing region presented in [11] is compared to the peak and midpoint catalytic factors predicted by BLIMPK in the present analysis for zone 3 at panels 7, 9, and 11, respectively. The recommended model was derived from the STS-5 C742 highly catalytic measurements on the left wing tile sensor locations and the STS-2 and -3 partially catalytic measurements at the same locations. The BLIMPK catalytic factor predictions for the two wing catalytic tiles on STS-5 match very well with the recommended model as do the peak catalytic factors at panels 7 and 9 from the STS-107 trajectory. The midpoint catalytic factor predictions at all the panels

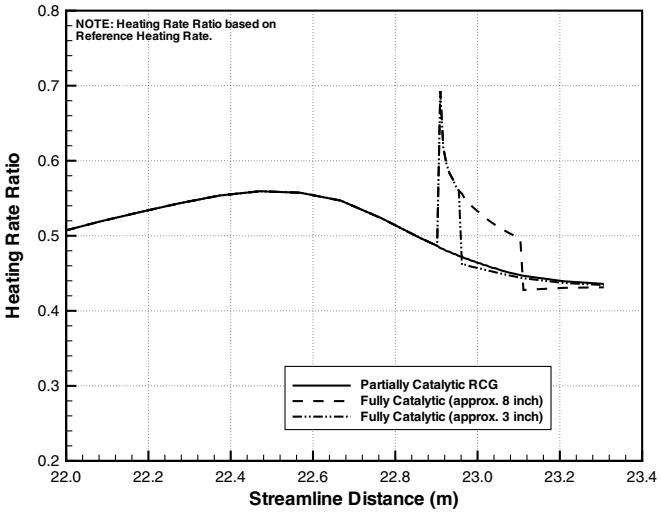

a) Catalytic length sensitivity study results for STS-107 Mach 18 Panel 9, Zone 3

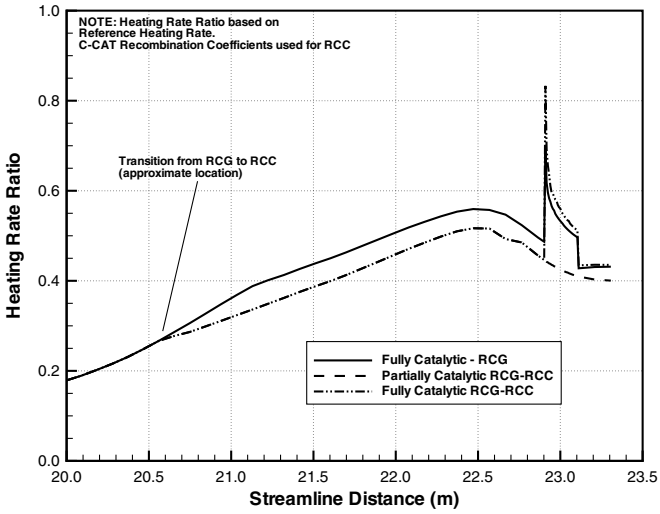

b) Recombination coefficient sensitivity study results for STS-107 Mach 18 Panel 9, Zone 3

Fig. 17 Results from sensitivity studies.

in zone 3 from the STS-107 trajectory are significantly lower as are the peak catalytic factors at panel 11. A limited amount of arcjet catalytic data[‡‡] obtained on a model placed in a wedge holder (flow parallel to surface) is also presented in Fig. 16 for comparison with the BLIMPK predictions and the flight correlations. This range of arcjet data resulted in factors of 1.47–1.66 based on a surface temperature increase of between 478–533 K, respectively, on the damaged RCC coating (assumed fully catalytic) compared to the undamaged RCC (partially catalytic). The analysis of these factors was the same as that reported in [20], by taking the ratio of the fourth power of the temperatures and assuming the surface emissivity was the same for damaged and undamaged RCC, as shown in Eq. (2). An undamaged RCC surface temperature of 1644 K was used, and a computed arcjet centerline (stagnation) enthalpy of 30.9 MJ/kg was determined.

E. Sensitivity Study

As noted in [20], the catalytic heating factor is sensitive to many different parameters, and it is important to understand how those parameters affect the chemical heating. For the STS-107 analysis,

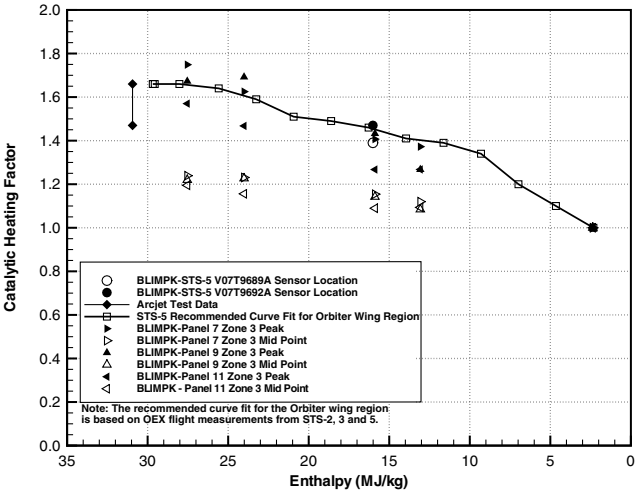

Fig. 16 BLIMPK peak and midpoint wing leading edge catalytic factors compared to the recommended model.

[‡‡]Information transmitted from A. Rodriguez and R. Lewis/NASA-JSC to W. Rochelle/ESCG-Jacobs, 2005.

catalytic location lengths were varied to determine if the size of a catalytic location had any effect on the overall bump factor. The recombination coefficients were also changed from RCG to C-CAT (RCC with type-A sealant) to observe the effect on the catalytic heating factors in the STS-107 wing leading edge analysis, although in this analysis, the flow would traverse RCG-coated tiles from the stagnation point, then the RCC wing leading edge, and then the catalytic damage site. In an actual flight case, a wing leading edge streamline would start at the RCC nose stagnation point, then flow over the RCG HRSI tiles, and then back over the RCC wing leading edge and over the catalytic damage.

Figure 17a contains the heating rate ratio result for the sensitivity study on the length of the fully catalytic location for panel 9, zone 3 at Mach 18 in the STS-107 trajectory. Figure 17a reveals that changing the length of the fully catalytic damage site from 20.30 to 7.60 cm has no effect on the peak catalytic heating or bump factor. Because the length has changed, however, there is an effect on the midpoint catalytic heating rate and the corresponding bump factor. The new midpoint distance is only 3.80 cm from the peak for the 7.60-cm catalytic region and has a bump factor of approximately 1.24, while the midpoint of the 20.30-cm catalytic region is 10.15 cm from the peak and has a bump factor of 1.14.

Figure 17b shows the heating rate ratio result for the sensitivity study performed on varying the recombination coefficients between RCG and RCC (C-CAT) for panel 9, zone 3 at Mach 18 in the STS-107 trajectory. Figure 17b reveals that the RCC recombination coefficients yield a lower partially catalytic heating rate while generating a higher fully catalytic heating rate at the damage site as seen in the STS-107 RCC nose analysis in Fig. 11. The higher fully catalytic heating rate and lower partially catalytic heating rate yield a larger catalytic bump factor (approximately 1.9 at the peak; 1.3 at the midpoint) than the RCG recombination coefficients (approximately 1.45 at the peak; 1.14 at the midpoint). This may not always be the case, because, as shown in Fig. 2a, the C-CAT recombination coefficients, and therefore the chemical heating, can be higher than RCG at lower (but still within flight range) temperatures.

F. Numerical Accuracy

Because the computer code used in the majority of analyses for this paper was the BLIMPK code, this section on numerical accuracy will focus primarily on that code. The details of the BLIMPK solution procedure and numerical accuracy of the code are discussed in [5]. Basically, the code uses a fourth-order Galerkin procedure where the main dependent variables and their derivatives in the normal direction (across the boundary layer) are related by Taylor series expansions. These variables are represented by connected

quadratics or cubics. A nodal network (matrix) is defined across the boundary layer with up to 15 nodal points for each distance step along a streamline. The series expansions are assigned values between each set of nodes. A higher accuracy is obtained in the solution by keeping the third and/or fourth terms in the series.

In BLIMPK, the conservation equations are integrated across each space between the nodal points in the boundary layer to simplify the normal derivative terms in the species and energy conservation equations [5]. A sparse matrix is formed, which has to be inverted only once for each station for linear series expansions and linear boundary conditions. However, the nonlinear equations and boundary conditions are solved with a Newton–Rhapson iteration procedure.

According to [5], BLIMPK can accurately calculate boundary layer flows with just 15 nodal points instead of 100–200 nodal points required by other lower order finite difference procedures. This is due to the higher-order spline representation of the boundary layer used in BLIMPK as opposed to the piecewise linear interpolation used in other procedures. To prevent nonconvergence, it is important to make good first guesses of primary variables such as wall enthalpy and wall species mass fractions. The program will iterate up to 100 times at a particular station before it stops, with the statement "nonconvergent output." The solution is sensitive to discontinuities in wall conditions such as surface pressure. However, if there is a gradual rise in pressure (such as in the Orbiter SSI region), but the nonequilibrium edge option is used with associated entropy decrements, the solution is usually convergent. In the present study, the solution was nonconvergent only for several cases on the Orbiter leeward side, where there was a possibility of flow separation.

Whenever there is nonconvergence at a particular station, adjustments are usually made in the BLIMPK input for initial guesses of wall enthalpy or wall species mass faction, or in the temperature tolerance for the radiation equilibrium temperature option. Usually, the temperature tolerance is set at 1 K; however, doubling this value will sometimes produce convergence. Also, convergence is usually produced by using connected cubic curve fits to represent primary variables of velocity ratio, total enthalpy, and elemental mass fractions rather than connected quadratics (which are more restrictive and used primarily for nearly blown-off boundary layers). Other methods to reduce nonconvergence of the solution include adjusting the initial guess of a wall temperature at a particular station, reducing the number of points across the boundary layer, and/or adjusting the point where the velocity ratio is fixed at a particular value (i.e., 0.95).

The BLIMPK code has been verified by various investigators over the years. The senior author of this paper was involved in an earlier study comparing BLIMPK-predicted heating rates on the Orbiter nose cap with outer mold line heating rates obtained from inner mold line radiometer temperature data for the STS-5 flight [8]. In that study, adjustments of catalytic recombination speed at the wall using BLIMPK were made to enable the boundary layer heating predictions to intersect the approximate midpoint of the flight data.

The present study and that of [20,40] verified the code by predicting good comparisons of BLIMPK heating predictions with STS-2, -3, and -5 centerline fuselage and wing flight data based on the RCG and C742 catalytic coatings. Arcjet data along a wedge simulating flow over the wing leading edge, which resulted in catalytic heating factors of 1.46–1.68 (shown in Fig. 16), were similar to some of the BLIMPK catalytic factors obtained on the wing areas at similar flow conditions in the present analysis.

The DPLR code, which was used to provide input to BLIMPK via the SRFTRACE code, uses a classical upwind finite volume formulation [32]. Inviscid fluxes are computed with a third-order monotone upstream-centered schemes for conservation laws (MUSCL) reconstruction scheme. The viscous terms are discretized with second-order central differencing. Like all total variation diminishing schemes, the achieved order of accuracy of the code is dependent on the particular mesh and flow features. For reentry simulations of the Orbiter, special care is taken in aligning the mesh with the bow shock of the vehicle to minimize the dissipative effects of MUSCL limiting.

The SRFTRACE code uses piecewise linear interpolation, which is second order accurate, to extract relevant data from the postprocessed CFD solutions. The metric coefficient computation is posed as an initial-value problem [cf. Eq. (13)] which is solved with a second-order explicit numerical integration technique.

The overall accuracy of both DPLR and LAURA heating rate predictions on the Orbiter smooth outer mold line (tile acreage) compared with STS-2 flight data was determined to be approximately 10%. This information was specified in the verification, validation, and accreditation report [41] in that the standard deviation (1 s) between CFD results and flight experiment was computed to be $\pm 9.63\%$.

IV. Conclusions

This paper presented the methodology and results of a two-layer surface catalytic heating analysis on the Orbiter RCG windward tile acreage and critical RCC nose cap, chin panel, and wing leading edge panels. Comparisons of the OEX STS-2, -3, and -5 flight data (with the highly catalytic C742 coatings) along the fuselage centerline and wing tile acreage were made with the BLIMPK heating predictions. The BLIMPK-predicted catalytic heating jumps compared very closely to the catalytic heating jumps derived from the OEX flight data. This method was extended to the RCC regions to calculate heating jumps for localized fully catalytic regions at assumed points of repair or damage on the critical RCC.

The highest midpoint catalytic heating factors calculated for the RCC regions were slightly over 2.0 for the nose cap leeward side and on the order of 1.5 for the windward side. Catalytic heating factors computed at RCC panels 7, 9, and 11 at six zones per panel for five freestream Mach numbers were lowest (on the order of 1.2) in regions where the heating rate was the highest (zones 3, 4). The catalytic factors were the highest on the leeward side (zones 5A, 6) and at zones 1 and 2 on the windward side where heating rates were lower.

The catalytic heating factors presented in this paper were recommended for use with potential repaired and damaged areas of RCC for real-time analysis for future flights in which in-flight repair would have to be made before reentry or flown as is.

Acknowledgments

J. J. Marichalar and W. C. Rochelle thank S. A. Bouslog (TPS NASA subsystem engineer, JSC ES3) for inspiring the concept of using catalytic heating overshoots to analyze damaged or repaired TPS surfaces, D. M. Curry (JSC ES3) for long-term leadership in catalytic heating to Orbiter LESS surfaces, K. C. Wang (Boeing-Houston) for use of the AA2LCH code for early analysis of two-layer streamline inputs to BLIMPK, and J. A. Fredo (formerly of Lockheed Martin and ESCG) who scanned nearly all the STS-2, -3, -5 flight data and made numerous wing leading edge calculations and plots during the study. B. S. Kirk and C. H. Campbell thank D. Prabhu (Eloret Corporation) for solutions to the DPLR code used in the SRFTRACE/BLIMPK analyses, and M. J. Wright (NASA Ames Research Center) for development of the DPLR code which has been used in numerous Orbiter reentry CFD analyses since the Columbia accident.

References

[1] The Columbia Accident Investigation Board, "The CAIB Report—Volume I," http://caib.nasa.gov, Aug. 2003.

[2] Hartung, L. C., and Throckmorton, D. A., "Space Shuttle Entry Heating Data Book," Vol. I-STS-2, NASA RP 1191, Parts 1 and 2, 1988.

[3] Hartung, L. C., and Throckmorton, D. A., "Space Shuttle Entry Heating Data Book," Vol. I-STS-3, NASA RP 1192, Parts 1 and 2, 1988.

[4] Hartung, L. C., and Throckmorton, D. A., "Space Shuttle Entry Heating Data Book," Vol. I-STS-5, NASA RP 1193, Parts 1 and 2, 1988.

[5] Murray, A. L., "Further Enhancements of the BLIMP Computer Code and User's Guide," AFWAL TR-88-3010, June 1988.

[6] Kolodziej, P., and Stewart, D. A., "Nitrogen Recombination on High-Temperature Reusable Surface Insulation and the Analysis of its Effects on Surface Catalysis," AIAA Paper 87-1637, June 1987.

[7] Stewart, D. A., "Catalytic Surface Effects Experiment (CSE) for Space Shuttle," *Orbiter Experiments (OEX) Aerothermodynamics Symposium*, CP 3248, NASA, Part 1, April 1995, pp. 171–197.

[8] Ting, P. C., Rochelle, W. C., and Curry, D. M., "Comparison of Viscous Shock Layer and Boundary Layer Reentry Heating Techniques for Orbiter Nose Cap," AIAA Paper 86-1350, June 1986.

[9] Ting, P. C., Rochelle, W. C., and Curry, D. M., "Prediction of Aerodynamic Heating and Pressures on Shuttle Entry Air Data System (SEADS) Nose Cap and Comparison with STS-61C Flight Data," *Proceedings of the First International Conference on Hypersonic Flight in the 21st Century*, University of North Dakota, Grand Forks, ND, Sept. 1988.

[10] Rakich, J. V., Stewart, D. A., and Lanfranco, M. J., *Catalytic Efficiency of the Space Shuttle Heat Shield*, Vol. 85, AIAA Progress in Astronautics and Aeronautics, AIAA, New York, 1983, pp. 97–122.

[11] Marichalar, J. J., and Rochelle, W. C., "Catalytic Heating Factors as Derived from STS-2, STS-3, and STS-5 Orbiter Experiments (OEX) Flight Data," JSC 62579, Rev. A, Feb. 2006.

[12] Stewart, D. A., Rakich, J. V., and Lanfranco, M. J., "Catalytic Surface Effects of Space Shuttle Thermal Protection System During Earth Entry of Flights STS-2 Through STS-5," *Shuttle Performance: Lessons Learned*, CP-2283, NASA, 1983, pp. 827–845.

[13] Scott, C. D., "A Review of Non-Equilibrium Effects and Surface Catalysis on Shuttle Heating," *Shuttle Performance: Lessons Learned*, CP-2283, NASA, 1983, pp. 865–889.

[14] Stewart, D. A., Rakich, J. V., and Chen, Y. K., "Flight Experiment Demonstrating the Effect of Surface Catalysis on the Heating Distribution over the Space Shuttle Heat Shield," *Orbiter Experiments (OEX) Aerothermodynamics Symposium*, CP-3248, NASA, Part 2, April 1995.

[15] Scott, C. D., and Derry, S. M., *Catalytic Recombination/Space Shuttle Heating*, Vol. 85, AIAA Progress in Astronautics and Aeronautics, AIAA, New York, 1983, pp. 123–148.

[16] Rochelle, W. C., and Norman, I., "Review of Arc-Jet Aerothermal Environments," Rockwell International SE-TCS-95-099, Nov. 1995.

[17] Reynolds, D., Norman, I., Reyna, J., and Chao, D. C., "Plasma Arc Jet Test Results of Uncoated AVTEX and ENKA Reinforced Carbon-Carbon (RCC) for Transoceanic Abort (TAL) Landing Verification," Rockwell International SE-TSAT-90-101, Dec. 1990.

[18] Norman, I., Chao, D. C., and Reyna, J., "Plasma Arc Tests for RCC TAL Abort Verification Coated AVTEX Reinforced Carbon-Carbon (RCC) Results," Rockwell International SE-TSAT-90-038, June 1990.

[19] Reynolds, D., Norman, I., Reyna, J., and Chao, D. C., "Plasma Arc Jet Test Results of Coated AVTEX and ENKA Reinforced Carbon-Carbon (RCC) for Transoceanic Abort Landing (TAL) Verification Phase II," Rockwell International SE-TSAT-91-005, Feb. 1991.

[20] Marichalar, J. J., and Rochelle, W. C., "Recommended Catalytic Heating Factors for Nose Region Damage Assessment During Orbiter Reentry," JSC Orbiter Entry Aeroheating Note OEAN 0305-002.A, April 2005.

[21] Marichalar, J. J., Rochelle, W. C., Kirk, B. S., and Campbell, C. H., "BLIMPK/Streamline Suface Catalytic Heating Predictions on the Space Shuttle Orbiter," AIAA Paper 2006-0180, Jan. 2006.

[22] Scott, C. D., "Wall Catalytic Recombination and Boundary Conditions in Non-Equilibrium Hypersonic Flow—with Applications," *Proceedings of the Second Joint Europe/U.S. Short Course in Hypersonics*, U.S. Air Force Academy, Colorado Springs, CO, Jan. 1989.

[23] Scott, C. D., "Catalytic Recombination of Nitrogen and Oxygen on High-Temperature Reusable Surface Insulation," AIAA Paper 80-1477, July 1980.

[24] Stewart, D. A., "Surface Catalysis and Characterization of Proposed Candidate TPS for Access-to-Space Vehicles," NASA TM 112206, July 1997.

[25] Cheatwood, F. M., and Gnoffo, P. A., "User's Manual for the Langley Aerothermodynamic Upwind Relaxation Algorithm (LAURA)," NASA TM 4674, April 1996.

[26] McGrory, W. D., Stack, D. C., Applebaum, M. P., and Walthers, R. W., "GASP Ver. 3.1—The General Aerodynamic Simulation Program, AeroSoft, Inc., Aug. 1997.

[27] Tam, L. T., "LU-SGS Implicit Scheme for Entry Vehicle Flow Computation and Comparison with Aerodynamic Data," AIAA Paper 92-2671-CP, June 1992.

[28] An, M. Y., Wang, K. C., and Tam, L. T., "Computation of Inviscid Flowfield Around 3-D Aerospace Vehicles and Comparison with Experimental & Flight Data," AIAA Paper 93-0885, Jan. 1993.

[29] Wang, K. C., "An Axisymmetric Analog Two-Layer Convective Heating Procedure with Applications to Evaluation of Space Shuttle Wing Leading Edge and Windward Surface Heating," NASA CR-188343, 1994.

[30] Fay, J. A., and Riddell, F. R., "Theory of Stagnation Point Heat Transfer in Dissociated Air," *Journal of the Aeronautical Sciences*, Vol. 25, No. 2, Feb. 1958, pp. 73–85.

[31] Kirk, B., "A Tool to Extract Streamline Data from Navier-Stokes Solutions for Boundary-Layer Solutions" (to be published).

[32] Wright, M. J., Candler, G. V., and Bose, D., "Data-Parallel Line Relaxation Method for Navier-Stokes Equations," *AIAA Journal*, Vol. 36, No. 9, Sept. 1998, pp. 1603–1609.

[33] Alter, S., Reuther, J., and McDaniel, R., "Development of a Flexible Framework of Common Hypersonic Navier-Stokes Meshes for the Space Shuttle Orbiter," AIAA Paper 2004-2635, June–July 2004.

[34] Reuther, J., McDaniel, R., Brown, J., Prabhu, D., Saunders, D., and Palmer, G., "External Computational Aerothermodynamic Analysis of the Space Shuttle Orbiter at STS-107 Flight Conditions," AIAA Paper 2004-2281, June 2004.

[35] Saunders, D., "Curvature-Based Boundary Layer Edge Detection" (to be published).

[36] Tannehill, J. C., and Mugge, P. H., "Improved Curve Fits for the Thermodynamic Properties of Equilibrium Air Suitable for Numerical Computation Using Time-Dependent or Shock-Capturing Methods," NASA TR CR-2470, Oct. 1974.

[37] Rochelle, W. C., and An, M. Y., "Leading Edge Structural Subsystem (LESS) Entry Heating Study—Final Report. Vol. I—Methodology and Results," LESC-30453, May 1993.

[38] Curry, D., Rodriguez, A., and Fields, M., "Turbulent Heating on WLE for STS-114," 1 Aug. 2005. Retrieved 5 Jan. 2006, from http://www.nasa.gov/pdf/124111main_FD08_Ex_Pack.pdf, pp. 43–55.

[39] Alexander, E. C., Daniher, C. E., and Schlessinger, E. D. (eds.), "Space Shuttle Orbiter Entry Aerodynamic Heating 6.0 Loads Data Book," Rockwell International, STS88-0673, July 1988.

[40] Marichalar, J. J., and Fredo, J. A., "BLIMPK Catalytic Surface Heating Analysis on the Orbiter Wing Tile and RCC Wing Leading Edge," JSC-63232, Aug. 2005.

[41] External Aerothermal Analysis Team from NASA ARC, LaRC, and JSC, "Smooth Outer Mold Line Aerothermal Solution Database for Orbiter Windside Acreage Environments During Nominal Entry Conditions: Verification, Validation, and Accreditation Report," NASA JSC EG-SS-06-1, April 2005.

T. Lin
Associate Editor